Coupling Ferroelectricity with Spin-Valley Physics in Oxide-Based Heterostructures

Kunihiko Yamauchi,[1] Paolo Barone,[2] Tatsuya Shishidou,[3] Tamio Oguchi,[1] and Silvia Picozzi[2]
[1]ISIR-SANKEN, Osaka University, 8-1 Mihogaoka, Ibaraki, Osaka 567-0047, Japan
[2]Consiglio Nazionale delle Ricerche (CNR-SPIN), 67100 L'Aquila, Italy
[3]Department of Quantum Matter, ADSM, Hiroshima University, Higashihiroshima 739-8530, Japan
(Received 5 December 2014; revised manuscript received 15 April 2015; published 16 July 2015)

The coupling of spin and valley physics is nowadays regarded as a promising route toward next-generation spintronic and valleytronic devices. In the aim of engineering functional properties for valleytronic applications, we focus on the ferroelectric heterostructure $BiAlO_3/BiIrO_3$, where the complex interplay among a trigonal crystal field, layer degrees of freedom, and spin-orbit coupling mediates a strong spin-valley coupling. Furthermore, we show that ferroelectricity provides a nonvolatile handle to manipulate and switch the emerging valley-contrasting spin polarization.

DOI: 10.1103/PhysRevLett.115.037602 PACS numbers: 77.80.-e, 31.15.A-, 71.70.Ej, 85.75.-d

Technological advances in future electronics strongly rely on the investigation of quantum degrees of freedom of electrons. Besides electron charge, spin represents the most studied example due to its obvious connection with magnetic information storage. Spin may be also actively manipulated in devices based on spin-polarized transport [1], as in the prototypical spin FET proposed by Datta and Das [2]. Relativistic spin-orbit coupling (SOC), providing a link between the electron spin and orbital angular momenta, plays a central role in spin-polarization effects while preserving time-reversal symmetry. Such spin-polarization effects may appear even in centrosymmetric crystals [3,4], provided that the ions experiencing a strong SOC have an inversion asymmetric local environment, ultimately due to the localized character of SOC itself. In the absence of bulk inversion symmetry, SOC lifts the spin degeneracy, leading to spin-splitting phenomena known as Dresselhaus [5] and Rashba [6] effects. In the latter case, typically realized at interfaces or surfaces where inversion symmetry is structurally broken, the spin polarization is induced by an effective k-dependent magnetic field, whose strength can be modulated by applying an external electric field [2,7]. Alternatively, it has been recently understood that bulk Rashba-like effects can be realized in ferroelectric (FE) semiconductors [8], additionally providing a nonvolatile functionality (ferroelectricity) which is tightly bound to spin polarization and, as such, allows for its full-electric control [9].

Other degrees of freedom have been recently addressed, most notably valley pseudospin, labeling the degenerate energy extrema in the momentum space, which could be used in valleytronic devices exploiting the valley index of carriers to process information [10]. The research in this field has been boosted by the discovery of hexagonal 2D crystals [11,12], such as graphene and transition-metal dichalcogenide monolayers, displaying valleys at the corners (K points) of the Brillouin zone.

Various schemes have been proposed to generate valley currents in graphene, using line defects [13] or strain [14], and in biased dichalcogenide bilayers [15]. The detailed investigation of these materials has significantly contributed to the fundamental understanding of valley physics, leading to the identification of intrinsic physical properties associated with valley occupancy [16–18]. Interestingly, the symmetry properties of valley pseudospin imply that valley-contrasting physical quantities may emerge whenever inversion symmetry is broken [16,17]. In this respect, the possibility to permanently control the valley phenomenology via a nonvolatile FE polarization would open the path to novel device paradigms, analogous to the proposed FE Rashba semiconductors [9].

Most of the well-known FE materials are transition-metal oxides with perovskite structure. As was recently pointed out, the hexagonal geometry can indeed be realized in perovskite heterostructures $(ABO_3)_n/(AB'O_3)_2$ grown along the [111] direction, where the B' ions in the $(AB'O_3)_2$ bilayer sit on a corrugated graphenelike honeycomb lattice [19–22], as shown in Fig. 1. Recent technological developments [23] allow now to prepare such artificial layered heterostructures with atomic-scale precision [24,25], offering an unprecedented playground for the realization of oxide-based advanced electronics. In fact, these (111) superlattices could allow for the integration of functional properties typically found in oxides [26] with the spin-valley physics, which is expected to emerge in the hexagonal layered structure. Specifically, the "layer degree of freedom," naturally emerging in the bilayer geometry, can be described as a "pseudospin" up (down) labeling the state where the charge carrier is located in the upper (lower) layer, being related, therefore, to electrical polarization. Such a layer pseudospin is expected to couple with spin and valley pseudospin, possibly giving rise to exotic magnetoelectric effects [27].

Since the spin-valley contrasting properties can emerge when inversion symmetry is broken, in this Letter we focus

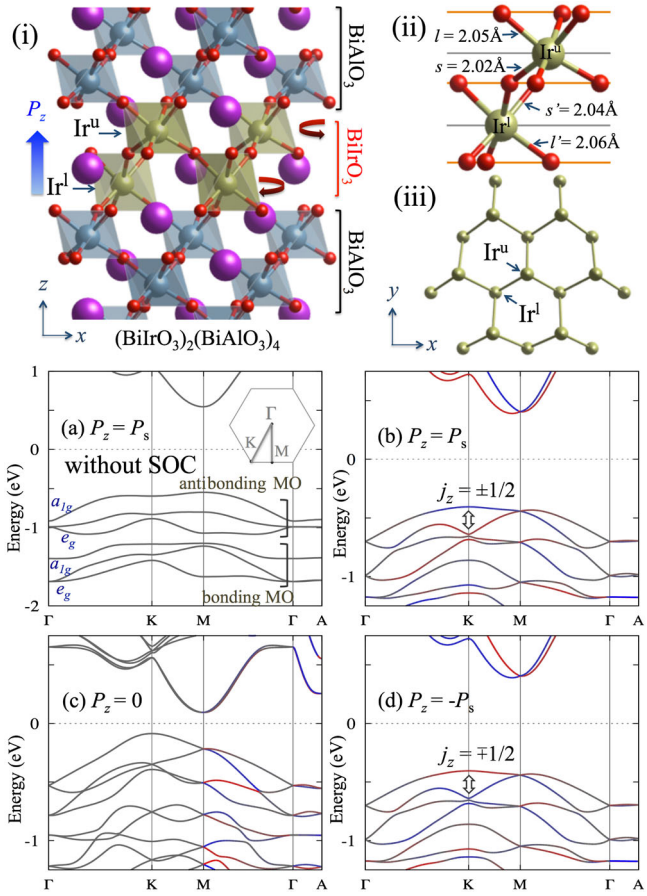

FIG. 1 (color online). (i) Multilayer structure of $(BiIrO_3)_2(BiAlO_3)_4$. Octahedral tilting and the polarization direction are shown by the arrows. (ii) Ir-O bond lengths in the bilayered structure and (iii) a top view of the corrugated honeycomb Ir lattice. Electronic band structure of FE $(BiIrO_3)_2(BiAlO_3)_4$ without SOC (a) and with SOC (b). With SOC, P is tuned to $P = 0$ in a PE parent structure (c) and to $P = -P_s$ (d), where P_s is the calculated spontaneous polarization. The s_z polarization is highlighted by the colors blue (up) and red (down). Spin splitting at VBM is indicated by the block arrows.

on the quest for FE spin-valley physics in perovskite oxides. As design criteria, a robust FE system with polarization perpendicular to the hexagonal bilayer is needed. Since the $BiFeO_3$-type rhombohedral crystal structure, displaying a [111] polar axis, is considered to be an ideal candidate to fulfill this criterion, we choose the nonmagnetic isostructural $BiAlO_3$ [28] recently synthesized, with a measured polarization $P_s \approx 27\ \mu C/cm^2$ and a high critical temperature, $T_c > 520°$ [29,30].

Aiming at a sizable spin splitting in a nonmagnetic system, in this study we propose the low-spin Ir^{3+} ($5d^6$) as a candidate B' ion due to its large atomic SOC. Density-functional-theory (DFT) calculations were performed using the VASP code with generalized gradient approximation–Perdew-Burke-Ernzerhof potential [31]. Technical details can be found in the Supplemental Material [32].

We first briefly summarize the outcome of our calculations for hypothetical bulk $BiIrO_3$. We found that it stabilized in the polar $R3c$ structure, with a calculated polarization $P_s = 70.6\ \mu C/cm^2$. Compared to the ideal perovskite structure, $BiIrO_3$ displays two main distortion modes, i.e., IrO_6 octahedral tilting and Bi-O polar distortion, the latter being responsible for the onset of ferroelectricity through the Bi lone-pair mechanism [40], alongside a compressive trigonal distortion. Ir^{3+}-$5d^6$ electrons stabilize in a low-spin state, whereas the trigonal distortion removes the degeneracy of fully occupied t_{2g} levels, which are split into a nondegenerate a_{1g} and twofold degenerate e'_g states (see the Supplemental Material [32]).

The bilayer structure displays a polar $P3$ symmetry, where Ir ions sit on a corrugated honeycomb lattice consisting of two trigonal layers intercalated by a single O layer, as shown in Figs. 1(i) and 1(iii). With respect to bulk $BiIrO_3$, an additional structural distortion develops, consisting in different distances of Ir layers from the central and the interfacial O layers, the latter showing, on average, longer Ir-O bonds [see Fig. 1(ii)]. The parent paraelectric (PE) structure, belonging to the $P321$ acentric (albeit nonpolar, due to $D_3 = 2C_3 + 3C'_2$ symmetry) space group, is reached by tuning the off centering of the central O layer with respect to the Ir ones, with other distortional modes showing minor changes. Therefore, spin-splitting effects may appear also in the acentric PE bilayer. Because of the C_3 site symmetry of Ir ions in both FE and PE structures, a built-in bulk Rashba-like (denoted as $R-1$) and Dresselhaus-like ($D-1$) effect can be anticipated, as arising from the local dipole field and the acentric environment, respectively [3]; in the presence of polar off centering, additional FE-modulated $R-1$ and $D-1$ spin polarizations should appear on top of such built-in effects.

The electronic band structure in the valence manifold mostly arises from the upper and lower Ir-(a_{1g}, e'_g) orbital states, forming molecular orbitals (MOs). Figures 1(a)–1(d) show the two bunches of d-electron bands, namely, the bonding and antibonding MOs arising from the d orbitals at two Ir sites. All of the bands are separated due to both trigonal crystal field (CF) and SOC-induced spin splitting. The valence band maximum (VBM) is at the K point; remarkably, all valence bands at K are spin polarized, displaying a large $s_z = 0.41\ \mu_B$ polarization at the VBM, whereas the s_x and s_y components are zero. Because of time-reversal symmetry relating the K and K' points, the VBM shows a positive (negative) spin polarization at the K (K') point, a manifestation of spin-valley coupling that emerges due to the polar distortion, as shown in Fig. 2(a). Interestingly, such valley-dependent spin polarization appears to strongly depend on the FE phase, being switched when the FE polarization of the heterostructure is reversed [Figs. 1(b) and 1(d)]. The size of the valley-spin polarization evolves proportionally to the size of the Bi-O off center, i.e., of P, as shown in Fig. 2(b), vanishing when

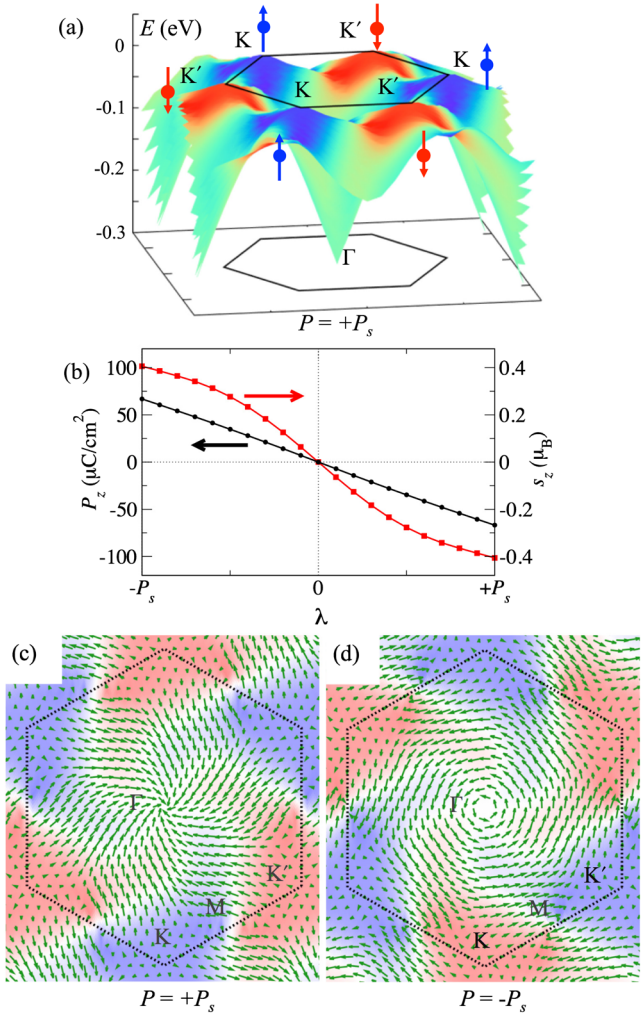

FIG. 2 (color online). (a) Spin valleys of $(BiIrO_3)_2(BiAlO_3)_4$: $\pm s_z$ polarization projected on the $E(k)$ curve of the VBM band. The top of E_{VBM} is set as 0 eV. (b) FE polarization P_z and spin polarization s_z of the VBM band at the K point as a function of the polar structural distortion λ. (c),(d) Spin texture of the VBM band for $+P_s$ and $-P_s$ crystal structures, respectively: the s_x and s_y components are shown by arrows, while the s_z component is plotted by the colors blue ($+s_z$) and red ($-s_z$) of the VBM band state. The first Brillouin zone is shown as a hexagon.

$P = 0$. In fact, even though a strong spin splitting is still visible in the PE band structure shown in Fig. 1(c), a finite s_z spin polarization is found only along the M-Γ line, being forbidden by the C_2' symmetries along the Γ-K line and at the valleys K, K'. However, a *hidden* valley-spin polarization can be identified when projecting the total s_z onto Ir ions belonging to different layers, hinting at an intrinsic strong spin-valley coupling (see the Supplemental Material [32]).

Eventually, a complex pattern of in-plane spin polarization is shown in Figs. 2(c) and 2(d), arising from the coexistence of several acentric distortions. The in-plane spin textures display the same chirality around the valleys, suggesting a substantial decoupling from the valley pseudospin. When the FE polarization is switched, a complete reversal of the spin-polarization texture is not realized, even though a clear switching of the chirality can be seen in Figs. 2(c) and 2(d); this suggests an interplay of FE-dependent and built-in R-1 and D-1 effects, the latter depending on the distortional modes which are almost unchanged when the polar off centering is tuned between opposite P_s's and persisting in the PE structure (see the Supplemental Material [32]). In summary, our *ab initio* calculations show a complex coexistence of valley-dependent and bulk Rashba-like (valley-independent) spin-polarization effects in bilayered $BiIrO_3$; remarkably, the spin-valley physics appears to be tightly bound to the FE distortion, emerging only in the polar structures.

The microscopic origin of the valley-spin polarization and its interplay with the FE polarization can be qualitatively grasped by considering a simplified tight-binding model $H = H_{hop} + H_{cf} + H_{soc}$ [19], describing t_{2g} electrons moving on a corrugated honeycomb lattice in the presence of both SOC and trigonal CF. The first term can be expressed as $H_{hop} = t_0 \sum_{\boldsymbol{r},\boldsymbol{r}'} \sum_{\beta,\beta'} T^{\beta\beta'}_{\boldsymbol{r}\boldsymbol{r}'} c^{\dagger}_{\boldsymbol{r}\beta} c_{\boldsymbol{r}'\beta'}$, where $\boldsymbol{r}$ and β label the lattice sites and the t_{2g} orbitals, respectively, while t_0 is taken to be the unit of energy and $T^{\beta\beta'}_{\boldsymbol{r}\boldsymbol{r}'}$ is a dimensionless structural factor containing both orbital and directional dependences [32,41]. The CF and SOC terms, with coupling constants Δ and λ, are given by $H_{cf} = \Delta \sum_{\boldsymbol{r}} \sum_{\beta\neq\beta'} c^{\dagger}_{\boldsymbol{r}\beta} c_{\boldsymbol{r}\beta'}$ and $H_{soc} = \lambda \sum_{\boldsymbol{r}} \boldsymbol{l}_{\boldsymbol{r}} \cdot \boldsymbol{s}_{\boldsymbol{r}}$, respectively, where $\boldsymbol{l}_{\boldsymbol{r}}$ ($\boldsymbol{s}_{\boldsymbol{r}}$) is the angular momentum (spin) operator. We will consider here only the effects of the polar distortion—in terms of the central O layer off centering δz—that affect both Ir-O bond lengths and directions and thus determine the explicit form of $T^{\beta\beta'}_{\boldsymbol{r}\boldsymbol{r}'}$, neglecting the more complex structural distortions unveiled by our realistic DFT calculations. The Hamiltonian can be conveniently recast on a symmetry-adapted basis where the trigonal CF term becomes diagonal, describing the t_{2g} splitting into a_{1g} and e_g' manifolds with a level separation 3Δ, while the on-site SOC displays the well-known expression found for p ($l = 1$) orbitals and given in Table I, the a_{1g} (e_g') states transforming as p_z (p_x, p_y) ones [32]. Interestingly, the symmetry properties of the a_{1g} states around the K valleys dictate a Dirac-like dispersion, namely,

$$H_{a_{1g}} = \frac{2t_0}{\sqrt{3}}(\tau k_x S_x + k_y S_y), \tag{1}$$

where $\tau = \pm 1$ is a valley index labeling K and K', and $\boldsymbol{S}$ denotes Pauli matrices for the layer pseudospin. Within this formulation, the analogies with graphenelike p-electron materials clearly emerge, the band splitting induced by the trigonal CF mimicking the sp^2 orbitals with σ, π character, whereas SOC may lead to the opening of an energy gap and to Rashba-like interactions in the corrugated honeycomb

TABLE I. Bulk symmetry [space group (SG)], atomic-site symmetry [site point group (SPG)], atomic SOC, and expected spin-polarization effects in coupled spin-valley 2D compounds. Following Ref. [3], R-1 and D-1 denote Rashba and Dresselhaus effects, while R-2 and D-2 denote the hidden spin polarizations due to the bulk IS. The electronic basis used for the SOC term is $\boldsymbol{c} = (p_x, p_y, p_z)$, comprising σ, π bands from sp^2 valence bonds, for p-electron systems, while it is $\boldsymbol{c} = (e^1_{(g)}, e^2_{(g)}, a_{1(g)})$ for d-electron MoS_2 (with a $BiIrO_3$ bilayer) as determined by the trigonal prismatic (octahedral + trigonal) CF.

	SG	SPG	SOC	Spin pol.
Graphene	$P6/mmm$	D_{3h}	$\boldsymbol{c}^\dagger_\alpha \times \boldsymbol{c}_\beta \cdot \boldsymbol{\sigma}_{\alpha\beta}$	D-2
Silicene	$P\bar{3}m1$	C_{3v}	$\boldsymbol{c}^\dagger_\alpha \times \boldsymbol{c}_\beta \cdot \boldsymbol{\sigma}_{\alpha\beta}$	R-2 and D-2
MoS_2	$P\bar{6}m2$	D_{3h}	$(c^\dagger_1 c_2 - c^\dagger_2 c_1)\sigma^z$	D-1
FE $BiIrO_3$	$P3$	C_3	$\boldsymbol{c}^\dagger_\alpha \times \boldsymbol{c}_\beta \cdot \boldsymbol{\sigma}_{\alpha\beta}$	R-1 and D-1

lattice due to spin-mixing terms coupling the π (a_{1g}) state with the σ (e'_g) manifold [42–44]. This is in striking contrast to the MoS_2 and d-electron dichalcogenide monolayers, where spin-up and spin-down states remain completely decoupled—even in the presence of SOC—due to the different trigonal prismatic CF acting on d orbitals (see Table I). On the other hand, oxygens in the oxide bilayer provide an additional way through which inversion symmetry in the graphenelike honeycomb lattice can be broken.

A standard down-folding procedure on the a_{1g} states near the $K(K')$ point allows us to derive an effective Hamiltonian for the valence bands, $H^{\text{eff}} = H^{\text{eff}}_0 + \delta z H^{\text{eff}}_1$, where the polar distortion has been included up to linear order in δz [32]. Here, H^{eff}_0 describes the low-energy electronic properties of the ideal (nonpolar) perovskite bilayer:

$$H^{\text{eff}}_0 = H_{a_{1g}} + \tau\sigma_z S_z \delta_0 + \lambda_R(\sigma_x k_y - \sigma_y k_x) S_z, \qquad (2)$$

where $\boldsymbol{\sigma}$ denotes the spin Pauli matrices, while δ_0 and λ_R are effective parameters depending on hopping amplitude t_0, atomic SOC, and trigonal CF [45]. As was anticipated before, Eq. (2) coincides with the low-energy model that has been derived for 2D atomic crystals with trigonal symmetry as silicene [44]. The second term describes the well-known spin-valley-layer coupling [42–44], which is responsible for the opening of a gap in the valence manifold. The last term describes a *layer-dependent* Rashba-like coupling which arises from the SOC-induced mixing of spin-up and spin-down states mediated by interorbital hoppings in the corrugated honeycomb lattice. Because of the centric symmetry of the ideal perovskite bilayer, no net spin polarization may appear; however, both the spin-valley-layer and the layer-Rashba coupling give rise to hidden layer-dependent spin polarizations (see the Supplemental Material [32]). In the presence of the polar distortion modeled by the central O layer off centering, the low-energy electronic properties are further described by

$$\begin{aligned} H^{\text{eff}}_1 = {} & E_z S_z + B_z \tau\sigma_z + \alpha(\tau S_x \sigma_y + S_y \sigma_x) \\ & + \lambda_{R1}[(S_x\sigma_x - \tau S_y \sigma_y)k_y + (S_y\sigma_x + \tau S_x \sigma_y)k_x] \\ & + \lambda_R(\sigma_x k_y - \sigma_y k_x), \end{aligned} \qquad (3)$$

where the additional effective parameters $E_z, B_z, \alpha, \lambda_{R1}$ can be expressed in terms of the tight-binding ones [46]. The coupling between spin and layer pseudospin described by H^{eff}_1, removing all of the degeneracies in the valence manifold, can be loosely regarded as a valley-dependent "magnetoelectric" interaction [27], explaining the emergence of a net spin polarization. It is also clear that, as highlighted by the linear dependence on the polar off centering δz, all of the coupling terms in Eq. (3) change sign upon reversal of the FE polarization, causing a global switching of the spin polarization. Specifically, the averaged *total* spin polarization can be derived at valleys $K(K')$, giving $s_z = \langle\sigma_z\rangle = \tau\delta z(E_z + B_z)/\sqrt{(E_z + B_z)^2 + (4\alpha)^2}$. Despite the minimal parametrization of the starting tight-binding model, the derived effective Hamiltonian clearly shows that the FE distortion is responsible for both a valley-spin polarization and an R-1 effect, both modulated by the size of the polar distortion.

In conclusion, we explored the possibility of engineering the spin-valley physics in FE transition-metal oxide heterostructures. We explicitly showed that the interplay of trigonal CF effects and SOC in (111) oxide bilayers leads to graphenelike low-energy electronic properties, thus allowing for the appearance of coupled spin-valley physics. Interestingly, the spin-valley-layer coupling term can be regarded as mediating an effective valley-dependent magnetoelectric interaction which manifests itself in complex patterns of spin and layer polarizations; when the polar distortion is induced by the oxygen-layer off centering, a large valley spin polarization, tuned by the FE polarization, develops, as we verified for a proposed candidate heterostructure comprising a robust FE $BiAlO_3$ and a bilayered $BiIrO_3$. The appearance of valley-contrasting properties and the magnetoelectric coupling brought in by the complex interplay of valley, spin, and layer pseudospin have been proposed as having important implications in valleytronic devices [10,17,27,47].

Even though the proposed material might not be suited for the optical and electrical generation of spin- and valley polarized carriers due to its indirect band gap and the nearly flat dispersion of the valence band maximum, we believe that our theoretical findings are more general, suggesting that the realization of spin-valley physics in oxide heterostructures is indeed possible. Our theoretical analysis further suggests that such a realization would allow, in principle, for larger effects (due to atomic SOC, which is typically large in $4d$ or $5d$ transition-metal ions), increased tunability (brought in by oxygens, both determining the trigonal CF splittings and mediating the hopping interactions), and the integration of additional

functionalities, such as ferroelectricity, which could be exploited in advanced next-generation electronic devices.

This work was supported by JSPS Kakenhi (Grants No. 22103004, No. 22103005, and No. 26800186). P. B. and S. P. acknowledge the Italian Ministry of Research through the project MIUR-PRIN "Interfacce di ossidi: nuove proprieta'emergenti, multifunzionalita'e dispositivi per l'elettronica e l'energia (OXIDE)".

K. Y. and P. B. contributed equally to this work.

[1] *Spin Electronics*, edited by M. Ziese and M. J. Thornton (Springer-Verlag, Berlin, 2001).
[2] S. Datta and B. Das, Appl. Phys. Lett. **56**, 665 (1990).
[3] X. Zhang, Q. Liu, J.-W. Luo, A. J. Freeman, and A. Zunger, Nat. Phys. **10**, 387 (2014).
[4] J. M. Riley, F. Mazzola, M. Dendzik, M. Michiardi, T. Takayama, L. Bawden, M. Granerød, M. Leandersson, T. Balasubramanian, M. Hoesch *et al.*, Nat. Phys. **10**, 835 (2014).
[5] G. Dresselhaus, Phys. Rev. **100**, 580 (1955).
[6] Y. A. Bychkov and E. I. Rashba, JETP Lett. **39**, 78 (1984).
[7] J. Nitta, T. Akazaki, H. Takayanagi, and T. Enoki, Phys. Rev. Lett. **78**, 1335 (1997).
[8] D. Di Sante, P. Barone, R. Bertacco, and S. Picozzi, Adv. Mater. **25**, 509 (2013).
[9] S. Picozzi, Front. Phys. **2**, 10 (2014).
[10] A. Rycerz, J. Tworzydlo, and C. W. J. Beenakker, Nat. Phys. **3**, 172 (2007).
[11] K. S. Novoselov, D. Jiang, F. Schedin, T. J. Booth, V. V. Khotkevich, S. V. Morozov, and A. K. Geimet, Proc. Natl. Acad. Sci. U.S.A. **102**, 10451 (2005).
[12] M. Xu, T. Liang, M. Shi, and H. Chen, Chem. Rev. **113**, 3766 (2013).
[13] D. Gunlycke and C. T. White, Phys. Rev. Lett. **106**, 136806 (2011).
[14] Y. Jiang, T. Low, K. Chang, M. I. Katsnelson, and F. Guinea, Phys. Rev. Lett. **110**, 046601 (2013).
[15] S. Wu, J. S. Ross, G.-B. Liu, G. Aivazian, A. Jones, Z. Fei, W. Zhu, D. Xiao, W. Yao, D. Cobden *et al.*, Nat. Phys. **9**, 149 (2013).
[16] X. Xu, W. Yao, D. Xiao, and T. F. Heinz, Nat. Phys. **10**, 343 (2014).
[17] D. Xiao, W. Yao, and Q. Niu, Phys. Rev. Lett. **99**, 236809 (2007).
[18] D. Xiao, G.-B. Liu, W. Feng, X. Xu, and W. Yao, Phys. Rev. Lett. **108**, 196802 (2012).
[19] D. Xiao, W. Zhu, Y. Ran, N. Nagaosa, and S. Okamoto, Nat. Commun. **2**, 596 (2011).
[20] J. L. Lado, V. Pardo, and D. Baldomir, Phys. Rev. B **88**, 155119 (2013).
[21] S. Okamoto, Phys. Rev. Lett. **110**, 066403 (2013).
[22] S. Okamoto, W. Zhu, Y. Nomura, R. Arita, D. Xiao, and N. Nagaosa, Phys. Rev. B **89**, 195121 (2014).
[23] D. P. Norton, Mater. Sci. Eng. R **43**, 139 (2004).
[24] G. J. H. M. Rijnders, G. Koster, D. H. A. Blank, and H. Rogalla, Appl. Phys. Lett. **70**, 1888 (1997).
[25] D. Hirai, J. Matsuno, and H. Takagi, Appl. Phys. Lett. **3**, 041508 (2015).
[26] H. Y. Hwang, Y. Iwasa, M. Kawasaki, B. Keimer, N. Nagaosa, and Y. Tokura, Nat. Mater. **11**, 103 (2012).
[27] Z. Gong, G.-B. Liu, H. Yu, D. Xiao, X. Cui, X. Xu, and W. Yao, Nat. Commun. **4**, 2053 (2013).
[28] P. Baettig, C. F. Schelle, R. LeSar, U. V. Waghmare, and N. Spaldin, Chem. Mater. **17**, 1376 (2005).
[29] J. Y. Son, C. S. Park, and Y.-H. Shin, Appl. Phys. Lett. **92**, 222911 (2008).
[30] J. Zylberberg, A. A. Belik, E. Takayama-Muromachi, and Z.-G. Ye, Chem. Mater. **19**, 6385 (2007).
[31] G. Kresse and J. Furthmüller, Phys. Rev. B **54**, 11169 (1996).
[32] See Supplemental Material at http://link.aps.org/supplemental/10.1103/PhysRevLett.115.037602, which includes Refs. [33–39], for detailed description of DFT and model studies.
[33] J. P. Perdew, K. Burke, and M. Ernzerhof, Phys. Rev. Lett. **77**, 3865 (1996).
[34] J. Heyd, G. E. Scuseria, and M. Ernzerhof, J. Chem. Phys. **118**, 8207 (2003).
[35] R. D. King-Smith and D. Vanderbilt, Phys. Rev. B **47**, 1651 (1993).
[36] R. Resta, Rev. Mod. Phys. **66**, 899 (1994).
[37] J. Friedel, P. Lenglart, and G. Leman, J. Phys. Chem. Solids **25**, 781 (1964).
[38] D. J. Chadi, Phys. Rev. B **16**, 790 (1977).
[39] W. A. Harrison, *Electronic Structure and the Properties of Solids* (W.H. Freeman, San Francisco, 1980).
[40] J. B. Neaton, C. Ederer, U. V. Waghmare, N. A. Spaldin, and K. M. Rabe, Phys. Rev. B **71**, 014113 (2005).
[41] J. C. Slater and G. F. Koster, Phys. Rev. **94**, 1498 (1954).
[42] D. Huertas-Hernando, F. Guinea, and A. Brataas, Phys. Rev. B **74**, 155426 (2006).
[43] H. Min, J. E. Hill, N. A. Sinitsyn, B. R. Sahu, L. Kleinman, and A. H. MacDonald, Phys. Rev. B **74**, 165310 (2006).
[44] C.-C. Liu, H. Jiang, and Y. Yao, Phys. Rev. B **84**, 195430 (2011).
[45] The explicit expressions of the effective parameters, as derived in the Supplemental Material [32], are $\delta_0 = \lambda t_0^2[1+\lambda/(3\Delta+\lambda)]/C$ and $\lambda_R = \lambda t_0^2/(\sqrt{6}C)$, where $C = 9\Delta^2 - \lambda^2 - t_0^2$.
[46] The explicit expressions of the additional effective parameters, as obtained in Ref. [32], reads $E_z = -6\Delta t_0^2/C$, $B_z = 2\lambda t_0^2/C$, $\alpha = \sqrt{2}\lambda t_0(3\Delta-\lambda)/C$ and $\lambda_{R1} = \sqrt{2}\lambda t_0/[\sqrt{3}(3\Delta+\lambda)]$, where C has been defined in Ref. [45].
[47] K. Sakamoto, T.-H. Kim, T. Kuzumaki, B. Müller, Y. Yamamoto, M. Ohtaka, J. R. Osiecki, K. Miyamoto, Y. Takeichi, A. Harasawa *et al.*, Nat. Commun. **4**, 2073 (2013).